Multipole-Accelerated Capacitance Extraction Algorithms for 3-D Structures with Multiple Dielectrics

Keith Nabors and Jacob White, *Member, IEEE*

Abstract—**This paper describes how to extend the multipole-accelerated boundary-element method for 3-D capacitance computation to the case where conductors are embedded in an arbitrary piecewise-constant dielectric medium. Results are presented to demonstrate that the method is accurate, has nearly linear computational growth, and can be nearly two orders of magnitude faster than the standard boundary-element method based on matrix factorization.**

I. Introduction

THE self and coupling capacitances associated with integrated-circuit interconnect and packaging are becoming increasingly important in determining final circuit performance and signal integrity. This has increased interest in computationally efficient procedures for determining capacitances of general three-dimensional structures. One recently developed approach to capacitance computation, the multipole-accelerated boundary-element method, can accurately analyze complex structures extremely efficiently [1], [2], provided it can be assumed that the dielectric is homogeneous. For realistic problems, however, the dielectric inhomogeneity can not be ignored. For example, integrated circuit interconnect consists of multiple layers of polysilicon or metal conductors, separated by conformal or space-filling insulators with very different dielectric constants. In packaging and off-chip interconnect, conductors typically pass through plastic or ceramic holders with large relative dielectric constants.

In this paper we describe how to extend the multipole-accelerated boundary-element method to the case where conductors are embedded in an arbitrary piecewise-constant dielectric medium. We start, in the next section, by reviewing the standard equivalent charge approach to including dielectric interfaces in boundary-element based three-dimensional capacitance calculations. In Section III, we show how this formulation allows for a multipole-accelerated iterative solution method. The method's utility is demonstrated in Section IV, where we examine results from our program, FASTCAP2, for several examples. The results presented demonstrate that the method is accurate, has nearly linear computational growth, and can be nearly two orders of magnitude faster than the standard boundary-element method based on direct factorization algorithms.

Manuscript received April 14, 1992; revised July 10, 1992. This work was supported by the Defense Advanced Research Projects Agency contract N00014-91-J-1698, the National Science Foundation contract (MIP-8858764 A02), and grants from I.B.M. and Digital Equipment Corporation. This paper was recommended by W. W.-M. Dai.

The authors are with the Research Laboratory of Electronics and the Microsystems Technology Laboratory, Department of Electrical Engineering and Computer Science, Massachusetts Institute of Technology, Cambridge, MA 02139.

IEEE Log Number 9205573.

II. Equivalent-Charge Formulation

To determine all the self and coupling capacitances of a structure with m conductors, the conductor surface charges must be computed m times, with m different sets of conductor potentials. In particular, if conductor i is raised to unit potential and the rest are set to zero, then the total charge on conductor i is numerically equal to conductor i's self capacitance. Furthermore, any other conductor's total charge is numerically equal to the negative of its coupling capacitance to conductor i.

Given the conductor potentials, the conductor surface charges can be computed using an equivalent charge formulation. In this formulation, surface charge layers are placed at the conductor-dielectric and dielectric-dielectric interfaces, with densities $\sigma_c(x)$ and $\sigma_d(x)$, respectively, and the problem domain is replaced with free space. These surface charges therefore produce a potential given by

$$\psi(x) = \int_{S_c} \sigma_c(x') \frac{1}{4\pi\epsilon_0 \|x - x'\|} dS', + \int_{S_d} \sigma_d(x') \frac{1}{4\pi\epsilon_0 \|x - x'\|} dS' \quad (1)$$

where S_c and S_d are the conductor-dielectric and dielectric-dielectric interface surfaces. The densities $\sigma_c(x)$ and $\sigma_d(x)$ are determined in this equivalent free space problem by insisting that $\psi(x)$ match the conductor potentials for the original problem at conductor-dielectric interfaces, and that the normal derivative of the potential satisfy

$$\epsilon_a \frac{\partial \psi_+(x)}{\partial n_a} - \epsilon_b \frac{\partial \psi_-(x)}{\partial n_a} = 0, \; x \in \epsilon_a, \epsilon_b \text{ interface} \quad (2)$$

at any point x on a dielectric-dielectric interface. Here n_a is the normal to the dielectric interface at x that points into dielectric a; ϵ_a, and ϵ_b are the permittivities of the

corresponding linear, isotropic dielectric regions; $\psi_+(x)$ is the potential at x approached from the ϵ_a side of the interface, and $\psi_-(x)$ is the analogous potential for the b side [3], [4].

2.1. Discretization Scheme

To numerically compute σ_c and σ_d, the conductor surfaces and dielectric interfaces are discretized into $n = n_c + n_d$ small panels or tiles, with n_c panels on conductor surfaces and n_d panels on dielectric interfaces as in Fig. 1. It is then assumed that on each panel i, a charge, q_i, is uniformly distributed. For each conductor surface panel, an equation is written which relates the potential at the center of that ith panel, denoted p_i, to the sum of the contributions to that potential from the n charge distributions on all n panels. For example, the contribution of the charge on panel j to the potential at the center of panel i is given by the superposition integral

$$\frac{q_j}{a_j}\int_{\text{panel } j}\frac{1}{4\pi\epsilon_0\|x_i - x'\|}\,da' \tag{3}$$

where x_i is the center of panel i, a_j is the area of panel j, ϵ_0 is the permittivity of free space, and the constant charge density q_j/a_j has been factored out of the integral. The total potential at x_i is the sum of the contributions from all n panels,

$$p(x_i) = P_{i1}q_1 + P_{i2}q_2 + \cdots + P_{ij}q_j + \cdots + P_{in}q_n \tag{4}$$

where

$$P_{ij} \triangleq \frac{1}{a_j}\int_{\text{panel } j}\frac{1}{4\pi\epsilon_0\|x_i - x'\|}\,da'. \tag{5}$$

Similarly, for each dielectric interface panel, an equation is written that relates the normal displacement-field difference at the center of that ith dielectric interface panel to the sum of the contributions to that displacement field due to the n charge distributions on all n panels. In particular, if panel i lies on the interface between dielectrics with permittivities ϵ_a and ϵ_b, then from (2),

$$\epsilon_a\frac{\partial p(x_{i_a})}{\partial n_i} - \epsilon_b\frac{\partial p(x_{i_b})}{\partial n_i} = 0. \tag{6}$$

Here, n_i is a normal to panel i, and x_{i_a} and x_{i_b} are x_i approached from the ϵ_a and ϵ_b sides of the interface, respectively. Substituting for p from (4) breaks (6) into a sum over all the panels,

$$D_{i1}q_1 + D_{i2}q_2 + \cdots + D_{ij}q_j + \cdots + D_{in}q_n = 0 \tag{7}$$

where

$$D_{ij} \triangleq (\epsilon_a - \epsilon_b)\frac{\partial}{\partial n_i}\frac{1}{a_j}\int_{\text{panel } j}\frac{1}{4\pi\epsilon_0\|x_i - x'\|}\,da',\ i \neq j \tag{8}$$

since if evaluation point j is not on panel i the limits $x_{i_a} \to x_i$ and $x_{i_b} \to x_i$ just replace the intermediate variables with x_i. Careful evaluation of the limits when $i = j$ leads to the important special case [5]

$$D_{ii} \triangleq \frac{(\epsilon_a + \epsilon_b)}{2a_i\epsilon_0}. \tag{9}$$

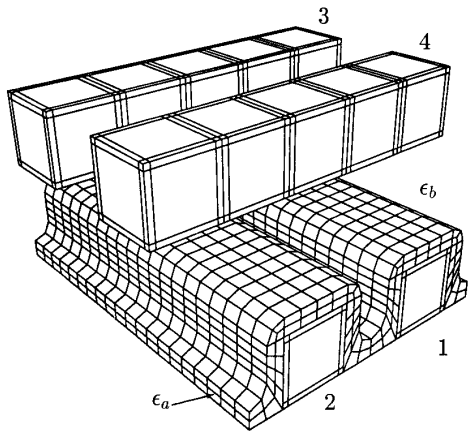

Fig. 1. The panels used to discretize a 2×2 dielectric-coated bus-crossing problem. The lower conductors' surfaces are discretized in the same way as the two upper conductors' surfaces.

Collecting all n equations of the form (4) and (7) leads to the dense linear system

$$\begin{bmatrix} P_{11} & \cdots & P_{1n} \\ \vdots & & \vdots \\ P_{n_c1} & \cdots & P_{n_cn} \\ D_{n_c+1,1} & \cdots & D_{n_c+1,n} \\ \vdots & & \vdots \\ D_{n1} & \cdots & D_{nn} \end{bmatrix}\begin{bmatrix} q_1 \\ \vdots \\ q_{n_c} \\ q_{n_c+1} \\ \vdots \\ q_n \end{bmatrix} = \begin{bmatrix} p_1 \\ \vdots \\ p_{n_c} \\ 0 \\ \vdots \\ 0 \end{bmatrix}. \tag{10}$$

A more convenient form of (10) is derived by rescaling the Equation (7) rows by $1/(\epsilon_a - \epsilon_b)$, which yields

$$\begin{bmatrix} P_{11} & \cdots & P_{1n} \\ \vdots & & \vdots \\ P_{n_c1} & \cdots & P_{n_cn} \\ E_{n_c+1,1} & \cdots & E_{n_c+1,n} \\ \vdots & & \vdots \\ E_{n1} & \cdots & E_{nn} \end{bmatrix}\begin{bmatrix} q_1 \\ \vdots \\ q_{n_c} \\ q_{n_c+1} \\ \vdots \\ q_n \end{bmatrix} = \begin{bmatrix} p_1 \\ \vdots \\ p_{n_c} \\ 0 \\ \vdots \\ 0 \end{bmatrix} \tag{11}$$

where E_{ij}, $i \neq j$, is just the normal electric field at x_i due to a unit charge on panel j, and is given by

$$E_{ij} \triangleq \frac{\partial}{\partial n_i}\frac{1}{a_j}\int_{\text{panel } j}\frac{1}{4\pi\epsilon_0\|x_i - x'\|}\,da',\ i \neq j. \tag{12}$$

Note that just like D_{ii}, E_{ii} is a special case, and is given by

$$E_{ii} \triangleq \frac{(\epsilon_a + \epsilon_b)}{2a_i\epsilon_0(\epsilon_a - \epsilon_b)}. \tag{13}$$

We will write this compactly as

$$\begin{bmatrix} P \\ E \end{bmatrix}[q] = \begin{bmatrix} p \\ 0 \end{bmatrix} \tag{14}$$

where $P \in \boldsymbol{R}^{n_c \times n}$ is the matrix of potential coefficients, $E \in \boldsymbol{R}^{n_d \times n}$ is the matrix of electric field coefficients, $q \in \boldsymbol{R}^n$ is the vector of panel charges, and $p \in \boldsymbol{R}^{n_c}$ is the vector of conductor-panel center-point potentials. Using

$$A \triangleq \begin{bmatrix} P \\ E \end{bmatrix}, \quad b \triangleq \begin{bmatrix} p \\ 0 \end{bmatrix} \tag{15}$$

gives

$$Aq = b \tag{16}$$

as the linear system to solve to for the conductor charge densities.

2.2. Matrix Solution

The standard approach to solving the $n \times n$ linear system (16) is to use Gaussian elimination, at a cost of order n^3 operations [4], [6]. For this reason, the equivalent charge formulation approach to capacitance calculation is frequently considered computationally intractable if the number of panels exceeds several hundred. To improve the situation, consider solving (16) using a conjugate-residual style iterative method like GMRES [7]. Such methods have the general form below.

Algorithm 1: GMRES algorithm for solving (16)
Make an initial guess to the solution, q^0.
Set $k = 0$.
do {
  Compute the residual, $r^k = b - Aq^k$.
  if $\|r\| < tol$, return q^k as the solution.
  else {
    Choose α's and β in
      $q^{k+1} = \sum_{j=0}^{k} \alpha_j q^j + \beta r^k$
    to minimize $\|r^{k+1}\|$.
    Set $k = k + 1$.
  }
}

If GMRES is used to solve (16), and assuming few iterations are required to achieve GMRES convergence, the dominant costs of the approach are calculating the n^2 entries of A from (5) and (12), and performing n^2 operations to compute Aq^k on each GMRES iteration. In the next section, we will describe an approach to computing Aq^k which eliminates the need to form most of A, and produces an approximation to Aq^k in order n operations [8].

It should be noted that when applied to solving (16), the standard GMRES algorithm frequently requires a large number of iterations to achieve convergence. If the number of GMRES iterations approaches n, then the minimization in each GMRES iteration requires order n^2 operations, and the whole algorithm uses order n^3 operations. This problem can be avoided easily through the use of the preconditioner described in [2], [9], which reduces the number of GMRES iterations required to achieve convergence with 1% error ($tol = 0.01$ in Algorithm 1) to well below n for large problems.

III. The Multipole Approach

The product Aq^k is, using (14),

$$Aq^k = \begin{bmatrix} Pq^k \\ Eq^k \end{bmatrix}. \tag{17}$$

Forming the product Pq^k is equivalent to calculating the potential at the conductor panel center points due to all the panel charges, and can be approximated directly in order n operations using the fast multipole algorithm [1], [2], [10]. Computing Eq^k is equivalent to calculating the normal electric field at all the dielectric panel center points and can also be approximated using a modification of the fast multipole algorithm. Below we give a brief description of the standard multipole algorithm for approximating Pq^k, and then give the approach for computing Eq^k.

3.1. Potential Evaluations

The key approximation employed in the multipole algorithm is the evaluation of potentials using multipole expansions. Consider evaluating the potential at d panel centers due to charges on another d panels as in Fig. 2. In a direct evaluation, a single panel's center-point potential is calculated using an explicit equation like (4). In the Fig. 2 case, d $P_{ij}q_j$ products are computed and added at a cost of d operations. Repeating the process for all d evaluation points requires d^2 operations.

When a cluster of panel charges are well-separated from a set of evaluation points, the potential at the evaluation points can be approximately computed in fewer than d^2 operations by making use of multipole expansions. A multipole expansion [10], [11] is a truncated series expansion of the form

$$p_i(r_i, \phi_i, \theta_i) \approx \sum_{j=0}^{l} \sum_{k=-j}^{j} \frac{M_j^k}{r_i^{j+1}} Y_j^k(\phi_i, \theta_i) \tag{18}$$

where (r_i, ϕ_i, θ_i) are the spherical coordinates of panel i's center point (the evaluation point) measured relative to the origin of the multipole expansion; $Y_k^j(\phi_i, \theta_i)$ are the surface spherical harmonics; l is the expansion order, and M_j^k are the multipole coefficients that are determined from the cluster of panel charges using

$$M_j^k \triangleq \sum_{i=1}^{d} \frac{1}{a_i} \int_{\text{panel } i} (\rho')^j Y_j^{-k}(\alpha', \beta')\, da'. \tag{19}$$

The use of the multipole expansion is illustrated in Fig. 3, where a single multipole expansion for the potential due to the d panel charges is used to compute the potential at d evaluation points. Since the expansion coefficients are computed once, but used d times, the cost of the coefficient computation may be neglected. Thus by using a multipole expansion, the cost of evaluating d

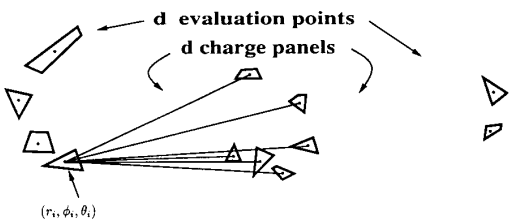

Fig. 2. The direct evaluation of the potential due to d panel charges at d points.

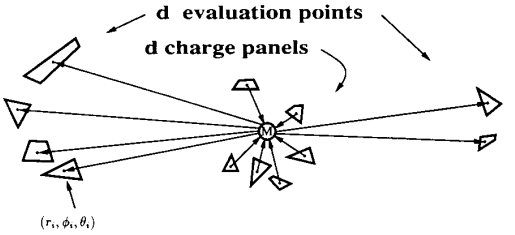

Fig. 3. The evaluation of the potential due to d panel charges at d points using a multipole expansion.

potentials from d panel charges is reduced to only order d operations.

Expansions can also be used to accelerate the computation of d potentials due to d panel charges when the *evaluation* points are clustered, if those points are well-separated from the panel charges. In this case, expansions are used to exploit the fact that the potential at any of the d evaluation points is roughly the same as the potential evaluated at the center of the cluster. Specifically, the potential due to the d panel charges can be represented by a local expansion with origin at the cluster's center, and the local expansion can be evaluated d times to determine the potential at d evaluation points. This situation is depicted in Fig. 4. Local expansions have the form

$$p_i(r_i, \phi_i, \theta_i) \approx \sum_{j=0}^{l} \sum_{k=-j}^{j} r_i^j L_j^k Y_j^k(\phi_i, \theta_i) \qquad (20)$$

where (r_i, ϕ_i, θ_i) are the spherical coordinates of i's center point measured relative to the origin of the multipole expansion, l is the expansion order, and L_k^j are the local expansion coefficients, which are calculated using the procedure in [1] and [10].

As the above examples make clear, multipole and local expansions are accurate when the evaluation points are well-separated from the panel charges being represented. This implies that for a general distribution, the potential due to nearby panel charges should be computed directly using (3). This result can then be summed with the contributions to the potential due to distant panels which, of course, can be represented using multipole or local expansions. Direct evaluations may also be used for small groups of distant panels, as multipole and local expansions are inefficient unless they are used to represent the effect of a large number of panel charges.

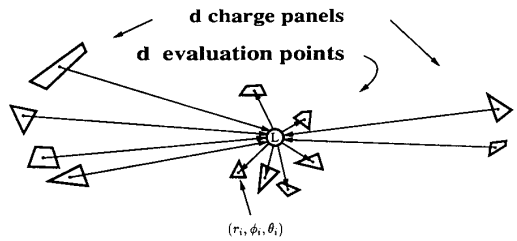

Fig. 4. The evaluation of the potential due to d panel charges at d points using a local expansion.

This short section is by no means intended to provide a complete description of the hierarchical multipole algorithm, only to make clear that the algorithm's efficiency stems from coalescing panel charges and evaluation points using multipole and local expansions. In addition, it should be noted that multipole-algorithm potential evaluations involve a combination of multipole and local expansion evaluations, and nearby-panel charge direct evaluations. A detailed description of the complete multipole algorithm is given in [10], and its use in the context of capacitance extraction is described in [1] and [2].

3.2. Electric Field Evaluations

A simple approach to using the multipole algorithm to compute normal electric fields, which are required for the equations associated with dielectric interfaces, is to use divided-differences. The fact that a surface charge will create a discontinuity in the electric field implies that when using divided-differences to compute the field at an evaluation point on a panel i, the field due to panel i's charge must be treated separately. Examining the ith row of the matrix E, as defined in (11) and (12), the diagonal entry relates the ith panel's charge to the normal electric field at the center of panel i, and the off-diagonal entries relate the charges on other panels to the normal electric field on panel i. Thus, the total normal electric field at panel i's center may be written as

$$E_{n_i} = E_{o_i} + E_{ii} q_i \qquad (21)$$

where E_{o_i} is the normal field due to all panels except panel i.

The field E_{o_i} can be approximated using divided-differences constructed from two potential evaluations as illustrated in Fig. 5. The potentials at two points x_a and x_b, both the same perpendicular distance away from the panel center x_i, combine to give

$$E_{o_i} \approx \frac{p(x_a) - p(x_b)}{h}. \qquad (22)$$

The potentials $p(x_a)$ and $p(x_b)$ can be computed, along with all the other evaluation point potentials, using the standard multipole algorithm. Therefore, the Eq^k product can be rapidly computed using the multipole algorithm followed by a multiply–subtract to form E_{o_i}, and then a multiply–add for the $E_{ii} q_i^k$ term.

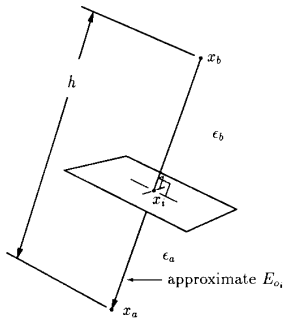

Fig. 5. The part of the normal electric field at the center of the dielectric panel due to distant charge panels can be approximated with a divided difference.

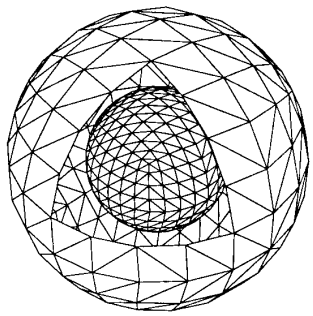

Fig. 6. The discretization used to compute the capacitance of a dielectric-coated sphere in free space. Some of the outer dielectric-boundary panels have been removed to show the inner conductor-surface panels.

An alternative to the divided-difference approach is to differentiate the multipole algorithm's expression for the potential analytically. As described in the previous section, a multipole-algorithm potential evaluation consists of multipole and local expansion evaluations combined with direct evaluations of the nearby-charge contributions, all of which may be analytically differentiated to obtain expressions for the normal electric field.

For the direct evaluations, the analytic differentiation of the potential coefficients gives the electric-field coefficients (12) and (13). Analytic differentiation of the multipole and local expansion components of the potential gives expansions for their contributions to the normal electric field at evaluation point x_i. In the context of (11), these electric field expansions contribute to the normal field at x_i by replacing many $E_{ij}q_j$ terms, leading to the same kind of efficiency as in the potential evaluation case. Details of the normal electric field calculation for both multipole and local expansions are given in the appendix.

In this way the multipole algorithm can be modified to calculate normal electric fields with a single evaluation rather than the two potential evaluations required by the divided-difference approach. Using the altered multipole algorithm also avoids the added inaccuracy inherent in a divided-difference approximation.

IV. Results

To demonstrate the efficiency and accuracy of the multipole-accelerated capacitance extraction algorithm for problems with multiple dielectrics, the capacitances associated with several test problems are calculated. Execution times are reported for large problems of practical interest and the computed capacitances are compared with analytic results and with results computed using the standard boundary-element method. All the results were obtained using our implementation of the algorithm in the program FASTCAP2, with the default 1% convergence tolerance ($tol = 0.01$ in Algorithm 1) and second-order expansions ($l = 2$ in (18) and (20)).

4.1. Coated Sphere

Using the dielectric-coated sphere of Fig. 6, FASTCAP2's accuracy is demonstrated by comparing its result to the exact result derived analytically. The inner conducting sphere of radius 1 m is coated by a 1-m thick dielectric layer with relative permittivity 2. The surrounding region is free space. By Gauss's Law, such a structure has capacitance 148.35 pF. The value calculated using FASTCAP2 applied to the discretization of Fig. 6 is 148.5 pF, well within 1% of the analytic value.

4.2. Bus Crossing

Somewhat more interesting from a practical standpoint is the bus-crossing structure of Fig. 1. The Fig. 1 problem is called the 2×2 bus-crossing problem and is representative of the 1×1 through 5×5 bus-crossings examined here. In all these problems the lower bus is covered with a layer of conformal dielectric with permittivity $\epsilon_a = 7.5\epsilon_0$ while the surrounding material has permittivity $\epsilon_b = 3.9\epsilon_0$. All the conducting bars have $1\text{-}\mu\text{m} \times 1\text{-}\mu\text{m}$ cross-sections, and all overhang and inter-conductor spacings are 1 μm. The conformal dielectric is nominally 0.25 μm thick.

The accuracy attained by FASTCAP2 is investigated using the Fig. 1 problem. The smallest coupling and self capacitances in the problem are calculated using FASTCAP2 and by Gaussian elimination applied directly to (16). Note that the Gaussian-elimination based algorithm is precisely the commonly used approach described in [4], and is a standard method for capacitance computation. The entries in Table I represent the capacitances associated with the top, rear conductor in Fig. 1. By default FASTCAP2 is configured to produce capacitances within 1% of those calculated using direct factorization, as is clearly the case here. Thus any error in the FASTCAP2 capacitances is dominated by discretization error rather than multipole approximation effects.

The program's execution speed for the four bus-crossing problems is compared to the speed of the standard direct method in Table II. The values in parentheses indicate extrapolated execution times corresponding to problems that could not be solved using the standard method due to excessive memory and time requirements. FASTCAP2's lower complexity leads to much lower exe-

TABLE I
COMPARISON OF CAPACITANCE MATRIX ENTRIES (IN fF) FOR THE FIG. 1 PROBLEM

	C_{31}	C_{32}	C_{33}	C_{34}
Direct	−0.2112	−0.2112	0.9854	−0.3200
FASTCAP2	−0.2113	−0.2112	0.9886	−0.3212

TABLE II
COMPARISON OF EXECUTION TIMES IN I.B.M. RS600 / 540 CPU MIN. VALUES IN PARENTHESES ARE EXTRAPOLATED

Problem	1 × 1	2 × 2	3 × 3	4 × 4
Panels	664	1984	3976	6640
Direct	1.4	41	(320)	(1400)
FASTCAP2	0.44	2.4	8.6	20

cution times even for moderate sized problems like the 2 × 2 bus crossing. In particular, in the time required to compute the capacitance of the 4 × 4 bus crossing problem using standard direct methods, FASTCAP2 can perform 70 such calculations.

FASTCAP2's execution time is shown to grow roughly linearly with mn, where m is the number of conductors and n is the number of panels. Fig. 7 is a plot of the FASTCAP2 execution times in Table II versus mn for the bus-crossing problems. The execution time data points lie close to the best-fit straight line, indicating roughly order mn complexity.

4.3. Backplane Connector

The analysis of the connector problem in Fig. 8 provides a further example of the kind of computation made possible by FASTCAP2. Connectors of this type must be analyzed carefully when considered for use in high-speed bus connections [12]. The U-shaped polyester body, with relative permittivity of 3.5, holds 16 pins with 0.65-mm × 0.65-mm cross-sections and 3.25-mm center-to-center spacings. Using a 9524-panel discretization, FASTCAP2 computes all the self and coupling capacitances for the pins in 30 CPU min on an IBM RS6000/540 (see also Table III). An identical analysis using standard Gaussian elimination algorithms requires roughly 1.5 CPU days on the same machine. The four pins in the center have the highest self capacitances: 0.547 pF. The lowest self capacitance is 0.481 pF and is attained by the four corner pins. The strongest coupling capacitances, slightly more than 0.2 pF, occur between pin pairs next to the sides of the connector body. By grounding four pins on a main diagonal and the four pins on the remaining parallel two-pin diagonals, the maximum signal-pin coupling capacitance is reduced to around 0.065 pF. These capacitances compare well with independently calculated values reported in [12].

4.4. DRAM Cells

Fig. 9 illustrates a second practical example, a simplified model of three adjacent DRAM cells in the 1-Mbit DRAM described in [13]. In Fig. 9(b), the dielectric interfaces are removed to show the conductors more clearly. Each cell consists of a bit line running across the cell, terminating in a via. In Fig. 9, the three-bit lines are elevated on the right side of the figure and run downward to the left where they are attached to the conical vias. The vias connect to the drains of MOS transistors formed by polycide word lines crossing the substrate at right angles to the bit lines and 0.01 μm above the substrate. The polycide word line that controls the transistors is the lower left word line in Fig. 9. The transistors' sources are all connected to the polycide cell plate, which is also 0.01 μm above the substrate. The dimples in the ground plane below the bit line vias model the capacitors formed by the depletion regions surrounding the drains of the bit cell

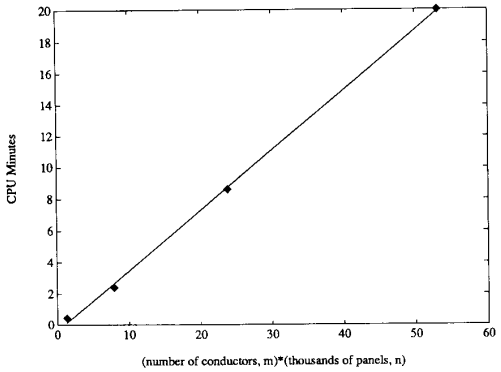

Fig. 7. Demonstration of the order mn complexity of FASTCAP2 using the four bus crossing execution times. Times are in CPU minutes on an I.B.M. RS6000/540.

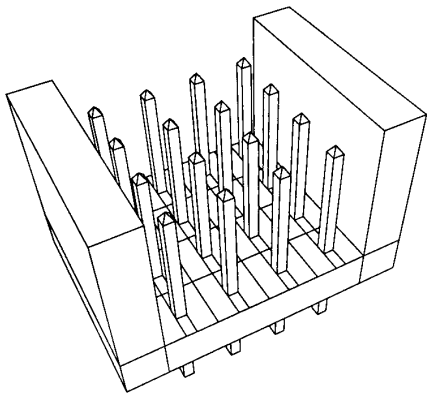

Fig. 8. The backplane connector example. The actual discretization used for the computation is much finer than the one illustrated.

TABLE III
FASTCAP2 TIMES IN IBM RS6000 / 540 CPU MIN

	DRAM	Connector
cond. panels	4881	6464
dielec. panels	1248	3060
total panels	6129	9524
CPU minutes	17	30

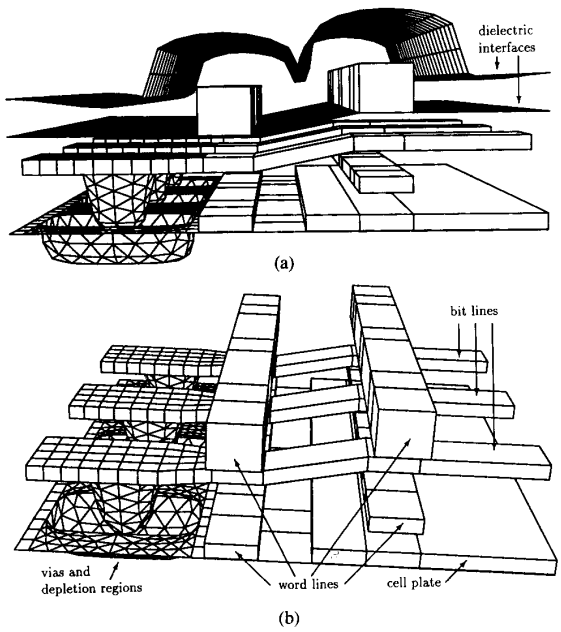

Fig. 9. (a) The complete DRAM model, and (b) with the dielectric interfaces removed for clarity.

MOS transistors. There are three other word lines passing through the cells at 0.7 μm (right), 1.8 μm (left), and 2.2 μm (right) above the substrate. All the lines are 1 μm wide and either 0.3 μm (top) or 0.9 μm (bottom) thick. The bit lines are spaced 2.4 μm apart and both sets of word lines are 2 μm apart. The upper, aluminum word lines are covered with a silicon nitride passivation layer with relative permittivity 7.0 and nominal thickness 0.7 μm. The passivation layer is represented by the two dielectric interfaces illustrated in Fig. 9(a). The material above the top interface is air, while below the lower interface silicon dioxide, with relative permittivity 3.9, is assumed.

Even though the DRAM example requires more than 6000 panels, FASTCAP2 was able to determine the capacitance matrix, given in Table IV, in less than 20 minutes (see Table III). The computed capacitances correspond reasonably with the measured data given in [13].

V. Conclusion

The multipole-accelerated capacitance extraction algorithm has been extended to problems with arbitrarily shaped, multiple-dielectric regions. The extended algorithm as implemented in FASTCAP2 has the same 1% accuracy and reduced time and memory requirements of the original algorithm [1], [2]. In particular, FASTCAP2 is fast enough to allow capacitance extraction of complex three-dimensional, multiple-dielectric geometries to be part of an iterative design process. It should be noted that no comparisons were made to finite-difference or finite-element based capacitance computation programs. The program FASTCAP2 is publicly available, and the authors hope this will facilitate completing such a study.

TABLE IV
Bit-Line Capacitance Matrix, fF

	near bit line	center bit line	far bit line
near bit line	2.11	−0.065	−0.007
center bit line	−0.065	2.12	−0.063
far bit line	−0.007	−0.063	2.10

Appendix
Normal Electric Field Formulas

This appendix presents the formulas used to evaluate the normal electric fields required to enforce dielectric-interface boundary conditions in the capacitance extraction algorithm. The formulas use the same multipole and local expansions which are used to calculate conductor panel potentials, effectively finding the gradient of the potential along each dielectric panel's normal. The multipole and local expansions used are expansions with real coefficients in the style of [11] and are described in more detail in [1].

A.1. Electric Fields From Multipole Expansions (M2E)

The contribution of an order l multipole expansion to the potential at the point (r, θ, ϕ) is

$$p_{mul}(r,\theta,\phi) = \sum_{n=0}^{l} \frac{1}{r^{n+1}} \sum_{m=0}^{n} \frac{(n-m)!}{(n+m)!} P_n^m(\cos\theta) \times \left[\bar{M}_n^m \cos(m\phi) + \tilde{M}_n^m \sin(m\phi) \right]. \quad (23)$$

If (r, θ, ϕ) is the spherical-coordinate center of a dielectric panel with unit Cartesian-coordinate normal $n = (n_x, n_y, n_z)$, then the multipole expansion (23) contributes

$$E_{mul} \triangleq n \cdot \nabla \left\{ \sum_{n=0}^{l} \frac{1}{r^{n+1}} \sum_{m=0}^{n} \frac{(n-m)!}{(n+m)!} P_n^m(\cos\theta) \left[\bar{M}_n^m \cos(m\phi) + \tilde{M}_n^m \sin(m\phi) \right] \right\} \quad (24)$$

to the electric field in the normal direction. Expanding the gradient in Cartesian coordinates using the chain rule leads to the directional derivatives

$$\frac{\partial}{\partial x} p_{mul}(r,\theta,\phi) = \frac{\partial p_{mul}}{\partial r}\frac{\partial r}{\partial x} + \frac{\partial p_{mul}}{\partial \theta}\frac{\partial \theta}{\partial x} + \frac{\partial p_{mul}}{\partial \phi}\frac{\partial \phi}{\partial x}; \quad (25)$$

$$\frac{\partial}{\partial y} p_{mul}(r,\theta,\phi) = \frac{\partial p_{mul}}{\partial r}\frac{\partial r}{\partial y} + \frac{\partial p_{mul}}{\partial \theta}\frac{\partial \theta}{\partial y} + \frac{\partial p_{mul}}{\partial \phi}\frac{\partial \phi}{\partial y}; \quad (26)$$

$$\frac{\partial}{\partial z} p_{mul}(r,\theta,\phi) = \frac{\partial p_{mul}}{\partial r}\frac{\partial r}{\partial z} + \frac{\partial p_{mul}}{\partial \theta}\frac{\partial \theta}{\partial z} + \frac{\partial p_{mul}}{\partial \phi}\frac{\partial \phi}{\partial z}. \quad (27)$$

Performing the dot product and rearranging gives

$$E_{mul} = \frac{\partial p_{mul}}{\partial r}\left(\frac{\partial r}{\partial x}n_x + \frac{\partial r}{\partial y}n_y + \frac{\partial r}{\partial z}n_z\right) + \frac{\partial p_{mul}}{\partial \theta}\left(\frac{\partial \theta}{\partial x}n_x + \frac{\partial \theta}{\partial y}n_y + \frac{\partial \theta}{\partial z}n_z\right) + \frac{\partial p_{mul}}{\partial \phi}\left(\frac{\partial \phi}{\partial x}n_x + \frac{\partial \phi}{\partial y}n_y + \frac{\partial \phi}{\partial z}n_z\right). \quad (28)$$

For the case $\sin\theta \neq 0$, derivatives obtained by implicit differentiation of the coordinate conversion rules

$$z = r\cos\theta;\ x = r\cos\phi\sin\theta;\ y = r\sin\phi\sin\theta \quad (29)$$

together with various derivatives of (23),

$$\frac{\partial p_{mul}}{\partial r} = \sum_{n=0}^{l}\frac{-(n+1)}{r^{n+2}}\sum_{m=0}^{n}\frac{(n-m)!}{(n+m)!}P_n^m(\cos\theta) \times\left[\overline{M}_n^m\cos(m\phi) + \tilde{M}_n^m\sin(m\phi)\right] \quad (30)$$

$$\frac{\partial p_{mul}}{\partial \theta} = \sum_{n=0}^{l}\frac{1}{r^{n+1}}\sum_{m=0}^{n}\frac{(n-m)!}{(n+m)!} \times\left[\frac{(n-m+1)}{\sin\theta}P_{n+1}^m(\cos\theta) - \frac{(n+1)\cos\theta}{\sin\theta}P_n^m(\cos\theta)\right] \cdot\left[\overline{M}_n^m\cos(m\phi) + \tilde{M}_n^m\sin(m\phi)\right] \quad (31)$$

$$\frac{\partial p_{mul}}{\partial \phi} = \sum_{n=0}^{l}\frac{1}{r^{n+1}}\sum_{m=0}^{n}\frac{(n-m)!}{(n+m)!}P_n^m(\cos\theta) \times\left[-m\overline{M}_n^m\sin(m\phi) + m\tilde{M}_n^m\cos(m\phi)\right] \quad (32)$$

are substituted into (28). The derivative of the associated Legendre function in (31) has been replaced using the identity [14]

$$\sin\theta\frac{d}{d\theta}P_n^m(\cos\theta) = (n-m+1)P_{n+1}^m(\cos\theta) - (n+1)\cos\theta P_n^m(\cos\theta). \quad (33)$$

After the substitutions (28) becomes

$$E_{mul} = \sum_{n=0}^{l}\frac{1}{r^{n+2}}\sum_{m=0}^{n}\frac{(n-m)!}{(n+m)!} \times\Big\{\{A_n\cos(m\phi)P_n^m(\cos\theta) + [F_n^m\cos(m\phi) + B^m\sin(m\phi)]P_{n+1}^m(\cos\theta)\}\overline{M}_n^m + \{[G_n\sin(m\phi) - B^m\cos(m\phi)]P_n^m(\cos\theta) + F_n^m\sin(m\phi)P_{n+1}^m(\cos\theta)\}\tilde{M}_n^m\Big\}, \quad \sin\theta \neq 0 \quad (34)$$

where

$$A_n \triangleq (n+1)\left[\frac{\cos\theta}{\sin\theta}(n_x\cos\phi\cos\theta + n_y\sin\phi\cos\theta - n_z\sin\theta) - (n_x\sin\theta\cos\phi + n_y\sin\theta\sin\phi + n_z\cos\theta)\right] \quad (35)$$

$$B^m \triangleq (n_x\sin\phi - n_y\cos\phi)\frac{m}{\sin\theta}; \quad (36)$$

$$F_n^m \triangleq \frac{(m-n-1)}{\sin\theta}(n_x\cos\phi\cos\theta + n_y\sin\phi\cos\theta - n_z\sin\theta);$$

$$G_n \triangleq (n+1)\left[\frac{\cos\theta}{\sin\theta}(n_x\cos\phi\cos\theta + n_y\sin\phi\cos\theta - n_z\sin\theta) - (n_x\sin\theta\cos\phi + n_y\sin\theta\sin\phi + n_z\cos\theta)\right]. \quad (37)$$

For the special case $\sin\theta = 0$, (35) is replaced by

$$E_{mul} = \sum_{n=0}^{l}\frac{-(n+1)}{r^{n+2}}P_n^0(\cos\theta)\overline{M}_n^0, \quad \sin\theta = 0. \quad (38)$$

This equation's derivation starts from (23) for the special case $\sin\theta = 0$ and then proceeds as when $\sin\theta \neq 0$, with special attention to simplifications in $P_n^m(\cos\theta)$ and $(d/d\theta)P_n^m(\cos\theta)$.

The normal electric field evaluation at $x_i = (r, \theta, \phi)$ uses either (34) or (38), as appropriate, to replace the $E_{ij}q_j$ products in (11) corresponding to the charge panels represented by the multipole expansion.

A.2. Electric Fields From Local Expansions (L2E)

The contribution of an order l local expansion for the potential at the point (r, θ, ϕ) is

$$p_{loc}(r,\theta,\phi) = \sum_{n=0}^{l}r^n\sum_{m=0}^{n}\frac{(n-m)!}{(n+m)!}P_n^m(\cos\theta) \times\left[\overline{L}_n^m\cos(m\phi) + \tilde{L}_n^m\sin(m\phi)\right]. \quad (39)$$

The multipole and local expansions differ only in the powers of r that multiply each term. This similarity allows a development analogous to that in the previous section which gives

$$E_{loc} = \sum_{n=0}^{l}nr^{n-1}\sum_{m=0}^{n}\frac{(n-m)!}{(n+m)!}\Big\{ \times\{A_n\cos(m\phi)P_n^m(\cos\theta) + [F_n^m\cos(m\phi) + B^m\sin(m\phi)]P_{n+1}^m(\cos\theta)\}\overline{L}_n^m + \{[G_n\sin(m\phi) - B^m\cos(m\phi)]P_n^m(\cos\theta) + F_n^m\sin(m\phi)P_{n+1}^m(\cos\theta)\}\tilde{L}_n^m\Big\}, \quad \sin\theta \neq 0. \quad (40)$$

for the normal component of the electric field due to the local expansion (39) evaluated at dielectric panel center (r, θ, ϕ). The weights A_n, B^m, F_n^m and G_n are given by (35)–(37) as in the multipole expansion case. When $\sin\theta = 0$ the normal field is

$$E_{loc} = \sum_{n=0}^{l} nr^{n-1} P_n^0(\cos\theta)\overline{L}_n^0, \quad \sin\theta = 0. \qquad (41)$$

As in the multipole case, the evaluation of the normal electric field at $x_i = (r, \theta, \phi)$ uses either (40) or (41), as appropriate, to replace the $E_{ij}q_j$ products in (11) corresponding to the charge panels represented by the local expansion.

ACKNOWLEDGMENT

The authors would like to acknowledge many helpful discussions with Prof. Stephen Senturia and Brian Johnson. They are also grateful to Khalid Rahmat for his help with the DRAM example and the Appendix, and to Songmin Kim for his help in implementing FASTCAP2.

REFERENCES

[1] K. Nabors and J. White, "Fastcap: A multipole accelerated 3-D capacitance extraction program," *IEEE Trans. Computer-Aided Design* vol. 10, pp. 1447–1459, Nov. 1991.

[2] K. Nabors, S. Kim, and J. White, "Fast capacitance extraction of general three-dimensional structures," *IEEE Trans. Microwave Theory Tech.*, vol. 40, pp. 1496–1506, July 1992.

[3] M. A. Jaswon and G. T. Symm, *Integral Equation Methods in Potential Theory and Elastostatics*. London: Academic, 1977.

[4] S. M. Rao, T. K. Sarkar, and R. F. Harrington, "The electrostatic field of conducting bodies in multiple dielectric media," *IEEE Trans. Microwave Theory Tech.*, vol. MTT-32, pp. 1441–1448, Nov. 1984.

[5] R. Kress, *Linear Integral Equations*. Berlin: Springer-Verlag, 1989.

[6] A. E. Ruehli and P. A. Brennan, "Efficient capacitance calculations for three-dimensional multiconductor systems," *IEEE Trans. Microwave Theory Tech.*, vol. 21, pp. 76–82, Feb. 1973.

[7] Y. Saad and M. H. Schultz, "GMRES: A generalized minimal residual algorithm for solving nonsymmetric linear systems," *SIAM J. Scientific and Statistical Computing*, vol. 7, pp. 856–869, July 1986.

[8] V. Rokhlin, "Rapid solution of integral equations of classical potential theory," *J. Computational Phys.*, vol. 60, pp. 187–207, Sept. 1985.

[9] S. A. Vavasis, "Preconditioning for boundary integral equations," in *Proc. Copper Mountain Conf. Iterative Methods*, Apr. 1992.

[10] L. Greengard, *The Rapid Evaluation of Potential Fields in Particle Systems*. Cambridge, MA: M.I.T. Press, 1988.

[11] E. W. Hobson, *The Theory of Spherical and Ellipsoidal Harmonics*. New York: Chelsea, 1955.

[12] W. Whitehead, "The role of computer models in connector standardization," in *Proc. 24th Annual Connector and Interconnection Technology Symp.*, pp. 103–110, 1991.

[13] Y. Konishi, M. Kumanoya, H. Yamasaki, K. Dosaka, and T. Yoshihara, "Analysis of coupling noise between adjacent bit lines in megabit DRAM's," *IEEE J. Solid-State Circuits*, vol. 24, pp. 35–42, Feb. 1989.

[14] W. Magnus and F. Oberhettinger, *Special Functions of Mathematical Physics*. New York: Chelsea, 1949.

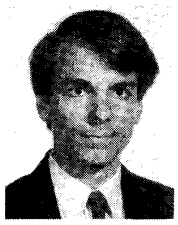

Keith Nabors received the B.E.S. degree from the Johns Hopkins University, Baltimore, Maryland, and the S.M. degree from the Massachusetts Institute of Technology. He is presently working towards the Ph.D. degree at the Massachusetts Institute of Technology.

His current interests are in numerical methods for circuit parameter extraction.

Jacob White (S'80–M'83) received the B.S. degree in electrical engineering and computer science from the Massachusetts Institute of Technology, Cambridge, and the S.M. and Ph.D. degrees in electrical engineering and computer science from the University of California, Berkeley.

He worked at the IBM T. J. Watson Research Center from 1985 to 1987, was the Analog Devices Career Development Assistant Professor at the Massachusetts Institute of Technology from 1987 to 1989, and is a 1988 Presidential Young Investigator. His current interests are in theoretical and practical aspects of serial and parallel numerical methods for problems in circuit design and fabrication.